DOI:
10.1039/C8SE00416A

Document Version
Peer reviewed version

The thermoelectrochemistry of the aqueous iron(II) / iron(III) redox couple: Significance of the anion and pH in thermogalvanic thermal-to-electrical energy conversion

Mark A. Buckingham,[a] Frank Marken,[b] Leigh Aldous[a,*]

[a] Department of Chemistry, Britannia House, King's College London, London, SE1 1DB, UK

[b] Department of Chemistry, University of Bath, Claverton Down, Bath BA2 7AY, UK

* Corresponding author: leigh.aldous@kcl.ac.uk

Manuscript submitted to *Sustainable Energy & Fuels*

Abstract

Thermogalvanic conversion of temperature gradients into electricity via a redox couple represents a potential method of waste energy harvesting, but inexpensive, effective and sustainable redox couples are required. In this study four aqueous Fe(II)/Fe(III) salt systems are considered, based upon ammonium iron sulphate, iron sulphate, iron trifluoromethanesulfonate and iron nitrate. A range of Seebeck coefficients were observed, from +0.18 ± 0.04 mV K^{-1} for ammonium iron (II/III) sulphate to +1.46 ± 0.02 mV K^{-1} for acidified iron (II/III) trifluoromethanesulfonate, both at a temperature difference of 20 K; notably these apparent Seebeck coefficients vary with temperature difference due to significant chemical equilibria. The iron (II/III) nitrate system generated the highest thermogalvanic power output. The systems were probed by cyclic voltammetry, pH, UV-Vis spectroscopy and electrochemical impedance spectroscopy, and two competing mechanisms noted, which strongly affect both the current output and Seebeck coefficient (*i.e.* potential output) of their thermoelectrochemical cells. Green and economic consideration are important aspects if these systems are to be employed in harvesting low-grade heat energy at a larger scale; iron nitrate and acidified iron sulphate were the most highly competitive systems.

Introduction

Temperature gradients can be converted directly into a flow of current (*i.e.* electricity) using the Seebeck effect; this corresponds primarily to conductors and semi-conductors.[1] A similar outcome can also be achieved using 'thermoelectrochemistry', whereby two electrodes at dissimilar temperatures and sharing a common redox active electrolyte results in a potential difference; connecting the electrodes results in a corresponding flow of thermogalvanic current.[1,2] The temperature dependence of the electrode potential is a fundamental parameter,[3] but is frequently referred to as the 'Seebeck Coefficient', or S_e, when discussed in the context of thermogalvanic conversion of temperature gradients to power.[1] In both cases, the thermodynamic driving force is the difference in entropy between the two halves of the redox couple, ΔS_{rc}, and the temperature difference, ΔT, such that:

$$S_e = {}^{\Delta V}/_{\Delta T} = {}^{\Delta S_{rc}}/_{nF}$$

Devices that exploit this are frequently referred to as liquid thermoelectrics,[4,5] thermoelectrochemical cells (thermocells)[5,6] or thermogalvanic cells.[1,2,4] The majority of systems have used aqueous electrolytes, with some exceptions.[4] While some systems have used metals and their ions for the redox couple, such as $Li^{+}|Li^{0}$ [6,7] and $Cu^{2+}|Cu^{0}$ [8,9] systems, most use two soluble redox states. In this context, the potassium ferricyanide / ferrocyanide ($K_3Fe(CN)_6$ / $K_4Fe(CN)_6$) redox couple is arguably the most extensively reported system, with aqueous S_e values of *ca.* -1.4 mV K^{-1}.[1,2,10]

Given the low potential generated by individual thermoelectrochemical cells, a solution is to combine multiple cells electrically in-series to increase the potential output. However, the need to avoid a thermal short circuit means that alternating cells should ideally have opposite signs for their S_e, so they can be arranged electrically in-series but thermally in-parallel; Al Maimani *et al.* reported the first detailed study of such liquid-based in-series system, using ferricyanide / ferrocyanide cells in-series with iron (II/III) sulphate cells.[5] Yang *et al.* also reported a similar system but using gelled electrolytes, and connecting ferricyanide / ferrocyanide cells in-series with iron (II/III) chloride cells.[10] In both studies the iron (II/III) cells were inferior to the ferricyanide / ferrocyanide cells.

Therefore iron (II/III) systems with positive S_e values are highly desirable, but these have not been investigated in detail. Fundamental work has been performed on measuring the ΔS_{rc} (and therefore S_e) of redox couples, but only at mM or μM levels.[11] The aqueous S_e of Fe^{2+} / Fe^{3+} was reported as *ca.* +1.8 mV K^{-1},[11] but only at ionic strength values below 0.2 M; above this the S_e rapidly dropped. Conversely, high power thermogalvanic devices require more concentrated systems (*i.e.* concentrations >1 M; ionic strengths frequently >3 M).[5] The theoretical S_e for Fe^{2+} / Fe^{3+} in water (calculated under standard conditions and in the absence of anions) has been reported as +1.175 mV K^{-1}.[3]

Regarding the thermoelectrochemistry of aqueous iron (II/III) chloride systems, Burrows reported a S_e of +0.6 mV K^{-1} for aqueous $FeCl_2$ / $FeCl_3$ in the presence of HCl.[2] Later, Yang *et al.* reported an S_e of +1.02 mV K^{-1} for aqueous $FeCl_2$ / $FeCl_3$ immobilised in PVDF with 10 w/w% HCl (up to ΔT = 20°C).[10] In ionic liquids, the chloride-based $[FeCl_4]^{2-}$ / $[FeCl_4]^-$ redox couple does not dissociate, and leads to an inverted S_e of −0.48 ± 0.02 mV K^{-1}.[12]

Regarding the thermoelectrochemistry of iron (II/III) sulphate systems, Al Maimani *et al.* reported S_e values in the range of +0.24 to +0.40 mV K^{-1} (from 1.4 M Fe^{2+} / 1.4 M Fe^{3+} to 0.0014 M Fe^{2+} / 0.0014 M Fe^{3+}, respectively), which could be increased to +0.54 mV K^{-1} with the addition of H_2SO_4 (all at ΔT = 50°C).[5] Later, Zhang *et al.* reported a S_e of +0.5 mV K^{-1} for aqueous 0.25 M $FeSO_4$ / 0.25 M $Fe[SO_4]_{1.5}$ for a ΔT of approximately 21°C, without acidification.[13]

A range of iron (II/III) systems have also been investigated in other systems, such as a range of ionic liquids.[12,14] The thermoelectrochemistry of a number of ferrocene/ferrocenium-based systems have been reported, all in ionic liquids, with S_e values ranging from -0.088 ± 0.02 mV K^{-1} to +1.67 ± 0.05 mV K^{-1}.[12,14–16] The 'un-complexed' Fe^{2+}/Fe^{3+} system, investigated as their $[NTf_2]^-$-based salts in an $[NTf_2]^-$-based ionic liquid, gave an S_e of +0.96 ± 0.04 mV K^{-1}.[12]

Therefore the S_e for aqueous Fe^{2+} / Fe^{3+} is expected to reach between *ca.* +1.2 mV K^{-1} [3] and *ca.* +1.8 mV K^{-1}.[11] To date, experimentally reported S_e values (for aqueous Fe(II) / Fe(III) salts) have fallen between +0.24 mV K^{-1} [5] and +1 mV K^{-1}.[10] The pH is clearly influential,[5] but, to the best of our knowledge, the nature of the anion has never been investigated in detail (in the context of thermogalvanic cells). Therefore this study reports an in-depth (thermo)electrochemical and spectroscopic study of four different aqueous Fe(II) /

Fe(III) systems, with a record high S_e of +1.46 ± 0.02 mV K^{-1} ultimately achieved for acidified Fe(II) / Fe(III) trifluoromethylsulfonate salts. The highly significant nature of the anion and pH is investigated. Preliminary comparisons of the economic and 'green' credentials are also evaluated, in the context of sustainable chemistry.

Experimental

Chemicals

All reagents were purchased from UK suppliers and were used as received, unless otherwise specified. These were ammonium Iron(II) sulfate hexahydrate (≥98%, Sigma Aldrich), ammonium Iron(III) sulfate dodecahydrate (≥99%, Sigma Aldrich), Iron(III) nitrate nonahydrate (≥99.95%, Sigma Aldrich), Iron(II) sulfate heptahydrate (99%, Acros Organics), Iron(III) sulfate pentahydrate (97%, Acros Organics), Iron(II) trifluoromethanesulfonate (≥85%, Sigma Aldrich), Iron(III) trifluoromethanesulfonate (90%, Sigma Aldrich), Nitric Acid (70%, Fisher Scientific), Sulfuric acid (1 M volumetric standard, Honeywell), Trifluoromethanesulfonic Acid (98+%, Alfa Aesar).

Synthesis of Iron(II) nitrate

Since Iron(II) dinitrate was not commercially available, it was synthesised *in situ* by preparing an aqueous solution containing 0.2 M Iron(II) chloride tetrahydrate (≥98%, Honeywell) and 0.4 M silver nitrate (99.5%, Acros Organics). This was stirred overnight until metathesis was complete, and the solution filtered using an Sartorius biotech Minisart® syringe filter to remove the silver chloride precipitate, to yield an aqueous solution of 0.2 M Iron(II) nitrate; cyclic voltammetry was used to confirm the absence of residual silver. Subsequently solid Iron(III) nitrate was dissolved to form a mixture of 0.2 M Iron(II) nitrate and 0.2 M Iron(III) nitrate, which was used directly. Since Iron(II) nitrate is known to slowly decompose,[17] these solutions were prepared immediately before use.

Thermoelectrochemistry

The thermoelectrochemical cell consisted of a Nylon 6,6 cylinder with an outer diameter of 18 mm, an inner diameter of 8 mm and a length of 8 mm (RS Components Ltd, UK). A machine cut lip 0.5 mm deep and 10 mm in diameter was introduced at either end using a Roland Modela MDX-40 CNC milling machine. Materials were machined using square-end mills between 1 and 3 mm in diameter. Into these were inserted two solid gold electrodes (1 mm thick discs with 10 mm diameter, from Surepure Chemetals, USA). The hollow cylinder was therefore filled with *ca.* 0.6 ml of electrolyte, and the gold electrodes were *ca.* 200 mm^2 and separated by 7 mm. Temperature control was maintained by directly contacting the gold discs with copper heat exchangers connected to RS-TX150 thermostatic circulator baths (Grant Instruments Ltd, UK). All measurements were made with the cell and electrodes arranged horizontally (*cf.* reference [8]). All potential and current measurements were performed using a Keysight B2901A Source Measure Unit (Keysight, UK). Current output was measured by setting a load resistance such that a constant pre-determined potential was generated, and the current output recorded for 10 minutes. Steady state output was achieved within a matter of seconds (Figure S2 (a) and (b)); the reported values are the average of the steady state current values recorded from 5 to 10 minutes.

Cyclic voltammetry

Cyclic voltammetric experiments were carried out using a PGSTAT 302N and NOVA software (Metrohm Autolab, the Netherlands). The electrochemical setup was an 1.6 mm diameter Au disc working electrode and a Pt wire counter electrode, *vs.* an Ag/AgCl (3 M NaCl) reference electrode (all BASi, USA), at a scan rate of 50 mVs^{-1}. All solutions contained 0.2 M of the Fe(II) salt and 0.2 M of the Fe(III) salt, in both the presence and absence of 1 M of the conjugate acid; no other supporting electrolyte was employed.

Electrochemical Impedance

Electrochemical Impedance was performed on solutions of 0.2 M of both Fe(III) and Fe(II) in the presence and absence of 1 M conjugate acid in the same setup as thermoelectrochemical measurements in the absence of supporting electrolyte. The impedance measurements were performed by a Solartron 1286/1250 system with Zplot/Zview software (Solartron, UK). The

impedance spectra were obtained at the equilibrium potential with a frequency range from 50,000 Hz to 1 Hz and with an amplitude of 20 mV

UV-Vis Spectroscopy

UV-Vis spectroscopy was performed using a Cary 100 UV-Vis and WinUV software (Agilent, UK) between 200 – 800 nm and with a UV-Vis crossover wavelength of 400 nm, using either ambient temperature (*ca.* 25°C) or an integrated Peltier temperature control block. Quartz cuvettes with a path length of 100 μm were used (FireflySci, USA). All spectrums were obtained using solutions containing 0.02 M of the Fe(II) salt and/or 0.02 M of the Fe(III) salt, in the presence and absence of 0.1 M of the conjugate acid.

pH measurement

The pH was measured using a digital pH meter (SciQuip Benchtop 9 Series pH and conductivity meter, SciQuip, UK). It was measured at ambient temperatures for solutions containing 0.2 M of the Fe(II) salt or 0.2 M Fe(III) salt, or both, in the presence and absence of 1 M of the conjugate acid.

Results and Discussion

Seebeck coefficient and Entropy of a range of iron salts

The temperature coefficient of the electrode potential, or apparent Seebeck coefficient (S_e) of four distinct Fe(II)/Fe(III) redox couples were first measured using non-isothermal thermoelectrochemical measurements, using 0.2 M of each redox state (total [Fe ion] = 0.4 M). Given the complex stoichiometry of the solid precursors, the $[NH_4]_2Fe(II)[SO_4]_2$ / $[NH_4]Fe(III)[SO_4]_2$ redox couple will be referred to in the simplified form '$[NH_4]FeSO_4$', the $Fe(II)SO_4$ / $Fe(III)[SO_4]_{1.5}$ as '$FeSO_4$', the $Fe(II)[NO_3]_2$ / $Fe(III)[NO_3]_3$ as '$FeNO_3$', and the $Fe(II)[CF_3SO_3]_2$ / $Fe(III)[CF_3SO_3]_3$ as '$FeCF_3SO_3$'. All were purchased as salts, with the exception of $Fe(II)[NO_3]_2$, which was prepared *in situ*, as described in the Experimental section. Attempts were made to measure the $Fe(II)Cl_2$ / $Fe(III)Cl_3$ system, but stable results could not be obtained.

Initially the S_e of all systems were measured at $\Delta T = 20°C$ ($T_{cold} = 15°C$, $T_{hot} = 35°C$, as a temperature range to represent exploiting waste radiative body heat.[18]) The resulting values are summarised visually in Figure 1, and are tabulated in the Table S1. Notably, the S_e varied significantly, from +0.18 ± 0.04 mV K^{-1} for $[NH_4]FeSO_4$ up to +1.35 ± 0.04 mV K^{-1} for $FeNO_3$; nearly an 8-fold difference.

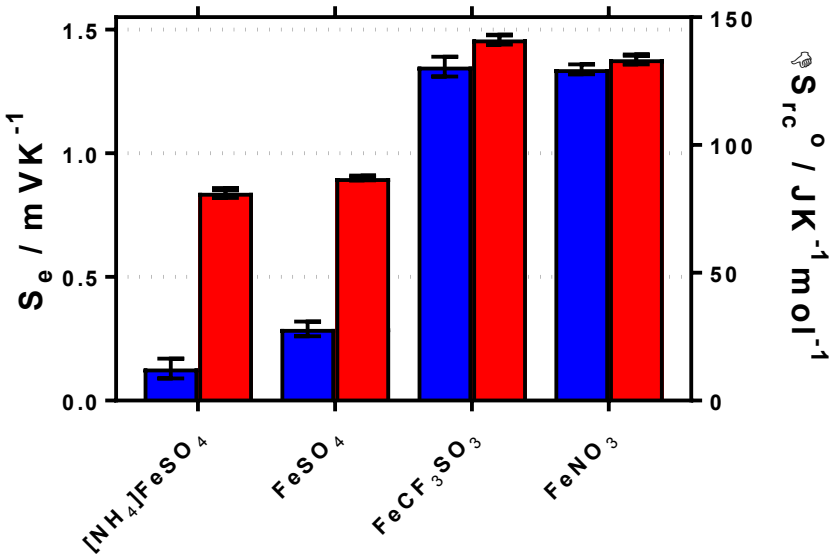

Figure 1 - Bar chart showing the Seebeck Coefficient (S_e) and Entropy values $\Delta S_{rc}°$ for various Fe(II)/Fe(III) systems, where the counter-ion is specified, in the presence (red) and absence (blue) of 1 M of the conjugate acid. All are reported at $\Delta T = 20°C$ ($T_{hot} = 35°C$ and $T_{cold} = 15°C$) and error bars are 1 SD of triplicate measurements. All Fe(II)/Fe(III) redox couples were present in a 50:50 ratio, and the solutions prepared to contain 0.2 M of the Fe(II) salt and 0.2 M of the Fe(III) salt (total redox active concentration 0.4 M).

Addition of 1 M of the conjugate acid of the anion to the systems resulted in significant increases in the S_e for both $[SO_4]^{2-}$-based systems, and the $[NH_4]FeSO_4$ increased up to +0.84 ± 0.02 mV K^{-1}; nearly a 5-fold increase. Acid addition resulted in only a minor increase in the S_e of the $FeNO_3$ and $FeCF_3SO_3$ systems (by up to 0.11 mV K^{-1}). Notably these systems have comparable S_e values (of inverted sign) to the S_e value of the *ca.* -1.4 mV K^{-1} widely reported for the $[Fe(CN)_6]^{4-}/[Fe(CN_6)]^{3-}$ system,[1,19] although comparable S_e values are not actually required to combine such systems electrically in-series.[5]

A maximum S_e value of *ca.* +1.8 mV K^{-1} was reported for the Fe^{2+}/Fe^{3+} redox system by Weaver *et al.*,[20] but this only applied for ionic strength values <0.2 M, which is equivalent to <17 mM of the $FeSO_4$ system. Above this ionic strength value the S_e value was reported to decrease.

Typically the S_e value should be independent of the temperature difference,[1] unless temperature-dependant equilibria is present.[15] For $[NH_4]FeSO_4$ a S_e of +0.18 mV K^{-1} was measured when $\Delta T = 20°C$, but this decreased to a S_e of +0.08 mV K^{-1} at $\Delta T = 5°C$, as shown in Figure 2(a); this highlights significant temperature-dependent dynamics were present in this system, and our use of the term 'apparent Seebeck coefficient'. The S_e of all the other systems (including acidified $[NH_4]FeSO_4$ in the presence of 1 M H_2SO_4) varied no more than 0.04 mV K^{-1} between $\Delta T = 5°C$ and $\Delta T = 20°C$, as highlighted in Figure 2(b) by the $[NH_4]FeSO_4$ and $FeNO_3$ systems (representative raw data shown in Figure S1 in ESI).

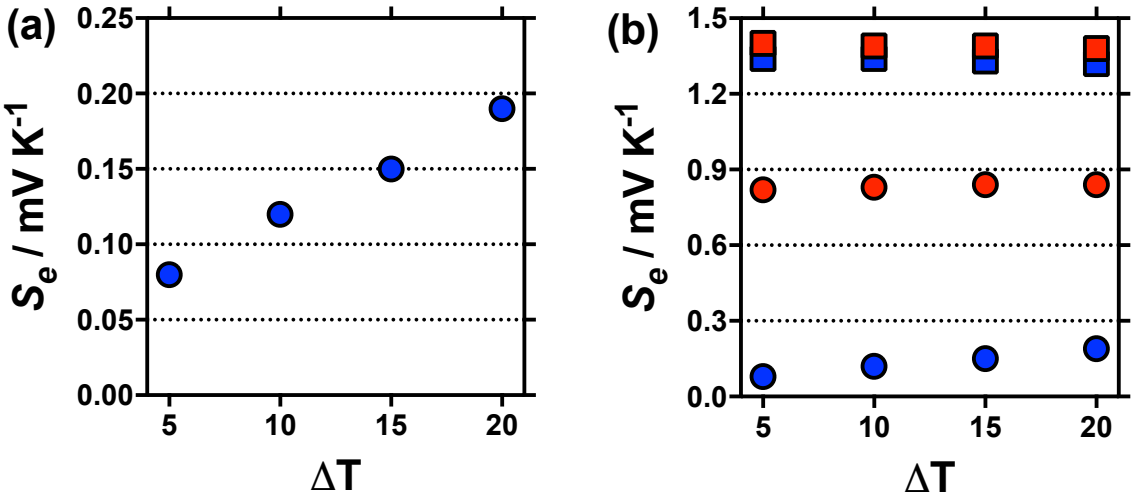

Figure 2 - Plots showing the variation in the apparent Seebeck Coefficient, S_e, against ΔT (T_{hot} = 35°C, T_{cold} = 15 to 30°C), for (a) ● un-acidified $[NH_4]FeSO_4$ system, and (b) ● $[NH_4]FeSO_4$ and ■ $FeNO_3$ systems, where blue is un-acidified and red is acidified; all other conditions match those in Figure 1. The high temperature sensitivity of the apparent S_e of the un-acidified $[NH_4]FeSO_4$ system against ΔT is immediately apparent, as is the relatively more minor variations in the other three systems.

The trend in S_e values across the redox couples can be rationalised in terms of acid-base equilibrium and ion pairing. The size and valence of the redox centre is highly influential in determining the S_e value,[16] and an ideal Fe^{2+} and Fe^{3+} redox couple is expected to have a high S_e value by virtue of their small size and high ionic charge.[11] However, it's well established that such iron salts undergo association with water and anions which will reduce their overall charge and therefore their redox entropy change;[11] this is especially true with Fe^{3+} and anions such as $[SO_4]^{2-}$, which can even form oligomeric $[Fe(SO_4)_n]^{3-2n}$ complexes.[21] The first step of these two competing equilibria are exemplified below using Fe^{3+} and $[SO_4]^{2-}$;

$$[Fe(H_2O)_6]^{3+} \rightleftharpoons [Fe(OH)(H_2O)_5]^{2+} + H^+ \qquad (1)$$

$$Fe^{3+} + [SO_4]^{2-} \rightleftharpoons [FeSO_4]^{+} \quad (2)$$

Both equilibria would be expected to demonstrate temperature dependence, as was experimentally observed here. For process (1), a decrease in pH would encourage more hexaaqua Fe^{3+} to be present (as opposed to species such as $[Fe(OH)]^{2+}$)[22] which would be reflected by an increase in the S_e value, as was observed experimentally for all systems. For process (2), this is highly anion dependant, with decreasing degrees of ion pairing expected to follow the trend $[SO_4]^{2-} >> [HSO_4]^{-} > [NO_3]^{-} \sim [CF_3SO_3]^{-}$ (based upon values published for iron solutions[21] and lanthanide salts[23]). It is notable that this trend also matches the experimentally observed trend in S_e. Additionally, acidification is not expected to influence $[NO_3]^{-}$ and $[CF_3SO_3]^{-}$, given the pK_a values of their conjugate acids are below that of water (-1.3[24] and -14.0,[25] respectively), whereas acidification of $[SO_4]^{2-}$ with an excess of H_2SO_4 would generate two $[HSO_4]^{-}$ (pK_a of $[HSO_4]^{-}$ = +2);[24] this would reduce ion pairing and thus increase the S_e value. Once again, this was also experimentally observed. Therefore measurements aimed at probing the relative contributions of processes (1) and (2) are discussed below.

pH and proton concentration

The pH of each solution was measured, for solutions containing 0.2 M of both the Fe(II) salt and Fe(III) salt, in the presence and absence of acid; the results are summarised in Figure 3(a). The inherent acidity of the iron solutions all fell within the pH range of *ca.* 1.75 ± 0.35; measuring the pH of the Fe(II) and Fe(III) salts separately demonstrated that the Fe(III) salts were responsible for at least 10-fold more inherent acidity (>1 pH unit lower) than the Fe(II) salts.

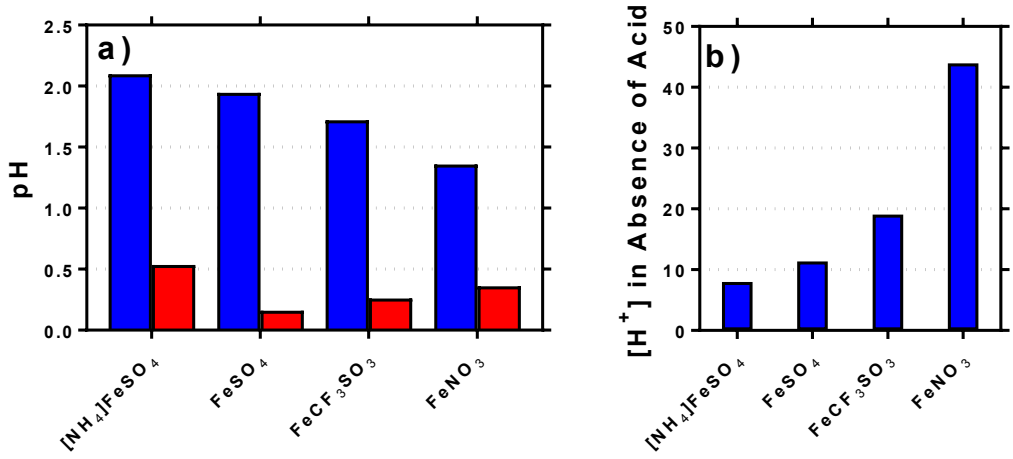

Figure 3 - Plots showing (a) the pH of the four different 0.4 M Fe(II)/Fe(III) systems, for their inherent pH (blue) and after addition of 1 M of their conjugate acid (red). Also shown in (b) is the concentration of protons, $[H^+]$, present in solution for the unacidified systems; the $[H^+]$ present indicates the extent to which process (1) (i.e. $[Fe(OH)(H_2O)_5]^{2+} + H^+$) occurs.

The concentration of acidic protons were calculated from the pH, and are shown in Figure 3(b). Notably, higher S_e values correlated with higher inherent proton concentrations; this is initially counterintuitive, since process (2) should reduce S_e. However, it is likely that process (1) and (2) are in competition, and therefore process (2) dominates for the $[SO_4]^{2-}$ systems; the higher valence of $[SO_4]^{2-}$ relative to $[OH]^-$ will result in a proportionately lower S_e, as was observed. This also explains why $[NH_4]FeSO_4$ had a lower S_e than $FeSO_4$, since the as prepared mixed valence solution of the former contained 2 $[SO_4]^{2-}$ per iron ion, whereas the latter contained only 1.25 $[SO_4]^{2-}$ per iron ion.

The highest concentration of protons observed corresponded to 45 mM for the $FeNO_3$ system, or *ca.* 23% of the 200 mM Fe(III) present. This has two implications; first is that the majority of species present are expected to be hydrated species (*cf.* $[Fe(H_2O)_6]^{3+}$), but process (1) will remove a significant minority of these species (*e.g.* as $[Fe(OH)(H_2O)_5]^{2+}$). The second is that since process (1) only influences the minority of redox-active species across the systems, process (2) is assumed to dominate the overall S_e trend observed. This was further probed spectroscopically.

UV-Vis Spectroscopy

All of the solutions containing 400 mM iron were strongly coloured, and changed significantly upon acidification; this is shown visually by the inserts in Figure 4, for (a) $FeSO_4$, and (b) $FeCF_3SO_3$. UV-Vis spectra demonstrated that this was almost entirely due to the Fe(III) salts, since none of the Fe(II) salts demonstrated appreciable absorption features

Figure S3; the exception was the nitrate salts, where absorbance of the $[NO_3]^-$ dominated both Fe(II) and Fe(III) features Figure S3.

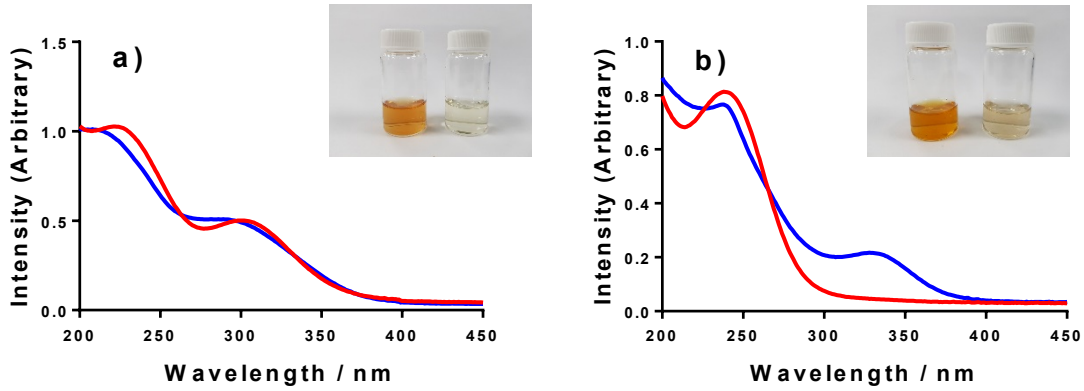

Figure 4 - UV-Vis spectra of (a) $FeSO_4$ and (b) $FeCF_3SO_3$ for concentration of 0.02 M of the Fe(II) and 0.02 M Fe(III) salts in the absence (blue) and presence (red) of 1 M conjugate acid. Inset – shows photos of these systems at the 0.4 M Fe(II)/Fe(III) concentration used elsewhere, in the absence (left in inset) and presence (right in inset) of 1 M conjugate acid.

The UV-Vis spectra of solutions containing both 20 mM Fe(II) and 20 mM Fe(III) salts were investigated as a function of added acid (0 mM and 100 mM of the conjugate acid) and temperature (5°C to 35°C); all significant spectral features correspond to the Fe(III) species.* All four iron systems displayed broad peaks centred on *ca.* 240 nm, which has been previously attributed to $[Fe(H_2O)_6]^{3+}$.[22] Absorption features at higher wavelengths have been attributed to complexes of Fe(III), such as $[Fe(OH)]^{2+}$;[22] in our results $FeSO_4$ had an additional feature at *ca.* 300 nm (Figure 4(a)), as did $[NH_4]FeSO_4$ (Figure S3(D)). Conversely, $FeCF_3SO_3$ had an additional absorption peak at *ca.* 340 nm (Figure 4(b)), as did $FeNO_3$ (Figure S3(C)). Addition of acid resulted in a sharpening of all peaks, consistent with a shift in a dynamic equilibrium, and in the case of $FeCF_3SO_3$ and $FeNO_3$ resulted in the complete loss of the absorption peak at *ca.* 340 nm (Figure 4(b) and Figure S3(C), respectively).

This allows us to conclude that the peak at *ca.* 340 nm corresponds to complex ions associated with process (1), such as $[Fe(OH)(H_2O)_5]^{2+}$; acidification with HCF_3SO_3 or HNO_3 shifts this equilibrium entirely to the left (to $[Fe(H_2O)_6]^{3+}$), resulting in the disappearance of this peak.

Upon acidification of $FeSO_4$ and $[NH_4]FeSO_4$ the feature at *ca.* 300 nm (in the 20 mM sample) shifted slightly but did not otherwise change. This initial peak likely corresponds to

* Despite using the smallest pathlength cuvette available (100 μm), the concentration had to be reduced to 20 mM Fe(III) to keep the absorbance within acceptable values.

species formed by process (2), such as $[FeSO_4]^+$; addition of a significant excess of H_2SO_4 failed to remove these adducts, and instead they likely persisted as $[FeHSO_4]^{2+}$ salts. Notably, since the extinction coefficients of these species are unknown, but are known to vary widely for different Fe(III)-adducts,[22] these results cannot be taken as quantitative. Such ion pairing interactions are also expected to be extremely concentration sensitive, given that acidification clearly had a more significant effect upon the 200 mM sample (shown in the insert in Figure 4(a)).

Further evidence that the different peaks found for $FeSO_4$ and $FeCF_3SO_3$ correspond to different processes was demonstrated by variable-temperature UV-Vis. Figure 5 displays UV-Vis spectra for these two systems measured between 5°C and 35°C; ion pairing (*i.e.* process (2)) would be expected to decrease with an increase in temperature, while acid-base dissociation (*i.e.* process (1)) would be expected to increase. In line with these expectations, the peak at *ca.* 300 nm for $FeSO_4$ decreased with increasing temperature, while the peak at *ca.* 340 nm for $FeCF_3SO_3$ increased. Furthermore, this temperature-sensitive equilibrium explains the significant temperature-dependence observed for the Seebeck coefficient of $[NH_4]FeSO_4$ (*cf.* Figure 2(a)), and the minor variation observed for the other systems.

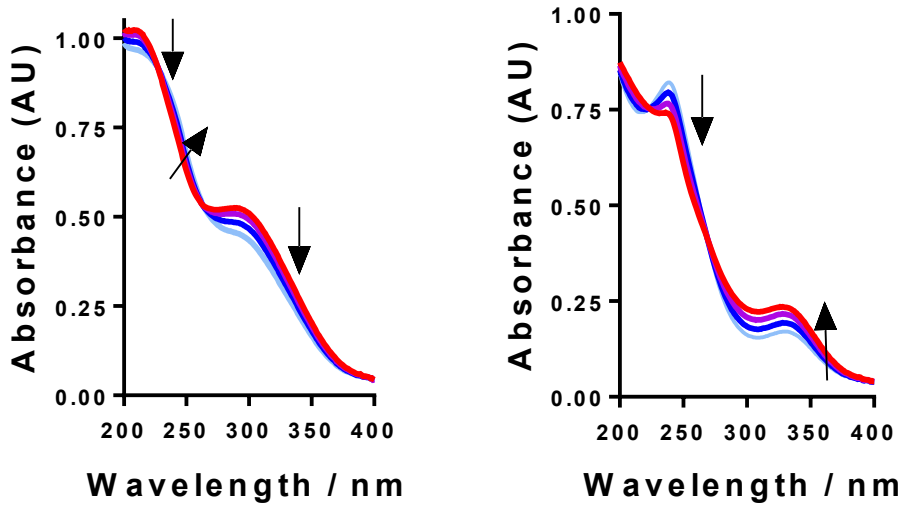

Figure 5 - UV-Vis spectra of (left) 40 mM $FeSO_4$ and (right) $FeCF_3SO_3$ recorded at temperatures of 5°C (light blue), 15°C, 25°C and 35°C (red); arrows indicate if absorption increased or decreased going from cold to hot.

Thermogalvanic power generation

Having characterised the properties of the systems, the thermogalvanic power produced by these redox systems were also measured at ΔT = 20°C. Figure 6 displays the power curves for the four systems, in the presence and absence of acid. The potential generated matched the trends observed for the S_e, as would be expected. The addition of acid can be seen to significantly increase the power density for all four systems (Figure 6).

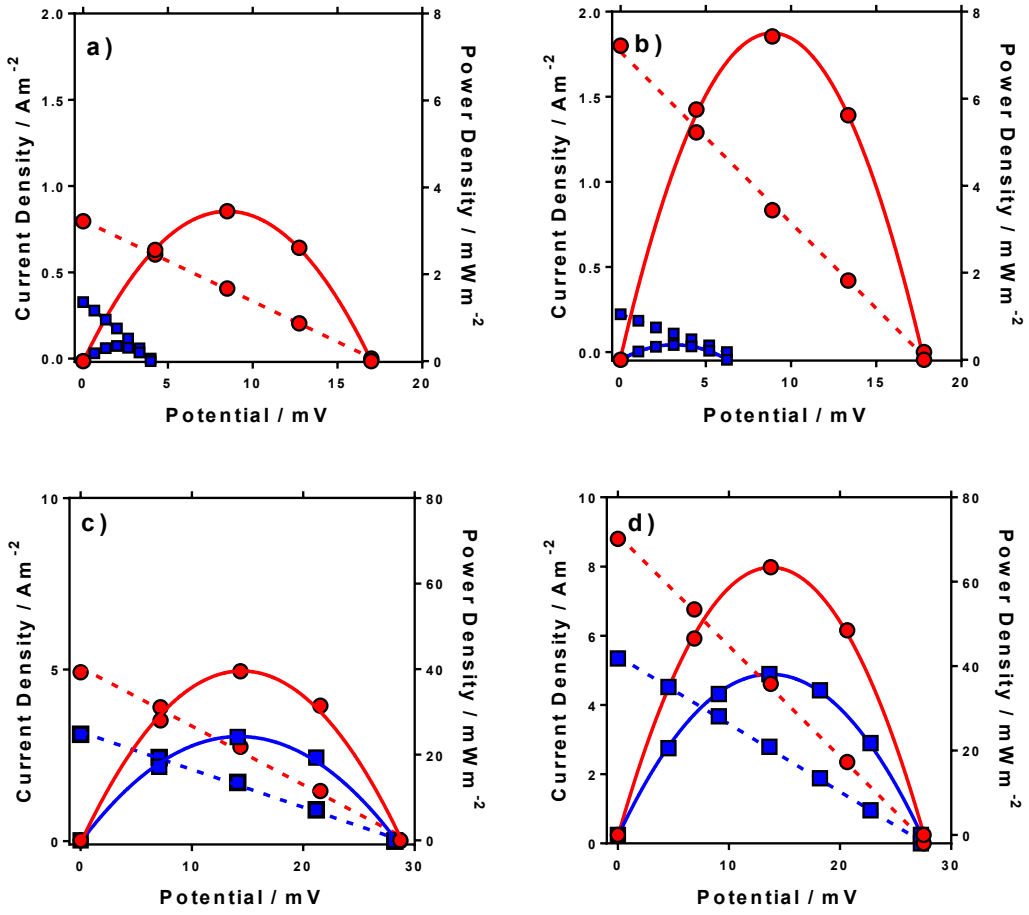

Figure 6 - Current and Power densities plots *vs* potential for (a) $[NH_4]FeSO_4$, (b) $FeSO_4$, (c) $FeCF_3SO_3$ and (d) $FeNO_3$. Current Densities are shown as dashed lines and Power Densities as solid lines, in the absence (blue) and presence (red) of 1 M conjugate acid at ΔT = 20°C.

The power curves for both $FeSO_4$ and $[NH_4]FeSO_4$ were strongly altered by the addition of acid; the increased potential leads to increased current and power, since the potential represents the thermodynamic driving force behind the process,[1] and acid-addition resulted in *ca.* 10 and 20-fold increases in the power output for the $[NH_4]FeSO_4$ and FeSO4 systems, respectively. Conversely, for $FeNO_3$ and $FeCF_3SO_3$, addition of acid had a minor effect upon the S_e but increased current by *ca.* 60% and 65% respectively, resulting in a *ca.* 60% and 65% increase in power output respectively.

In the case of $FeSO_4$ and $[NH_4]FeSO_4$, these systems are dominated by the ion pairing expressed by process (2). Acidification therefore removes the $[SO_4]^{2-}$ (by forming two $[HSO_4]^-$), and this acidification results in dramatic increases in the thermodynamic driving force (expressed as the S_e) by repressing process (2) and therefore the significant boost in power output shown in Figure 6. In the case of $FeNO_3$ and $FeCF_3SO_3$ process (2) is negligible and instead *ca* 10 - 20% of the Fe(III) salt is expected to have undergone process (1) (*cf.* Figure 3(b)). The reduced inherent S_e of $[Fe(OH)(H_2O)_5]^{2+}$ (relative to $[Fe(H_2O)_6)]^{3+}$) indicates these species would not have contributed significant current during thermogalvanic power generation. Since addition of acid removes these (*cf.* Figure 4(b)) this correlates with more thermogalvanically active species and therefore higher current, as seen experimentally.

It is important to note the scales on the power axis in Figure 6, which are an order of magnitude higher for $FeNO_3$ and $FeCF_3SO_3$ than for $FeSO_4$ and $[NH_4]FeSO_4$, highlighting the extremely significant role of the anion in thermogalvanic power generation. Interestingly, $FeNO_3$ resulted in a higher power output than $FeCF_3SO_3$, which could not be predicted by any of the earlier measurements; these systems were therefore investigated in more detail by cyclic voltammetry and impedance spectroscopy.

Cyclic Voltammetry and Impedance Spectroscopy

Cyclic voltammograms (CVs) were recorded at a gold electrode for the 400 mM mixed Fe(II/III) solutions, in the presence and absence of the conjugate acid. This represents extremely concentrated solutions and a general absence of any other supporting electrolyte, but is consistent with the solutions used elsewhere in this study. Figure 7 displays all of the CVs, and the relevant electrochemical parameters are summarised in Table S3. The trend in peak-to-peak separation somewhat correlated with the thermogalvanic power generated, and primarily the distinct difference between $[NH_4]FeSO_4$ / $FeSO_4$ systems and the $FeCF_3SO_3$ / $FeNO_3$ systems. However, these parameters are subject to the rate of electron transfer, ohmic drop and ionic migration, especially given the lack of excess supporting electrolyte. In order to evaluate the different components in more detail, impedance spectroscopy was employed.

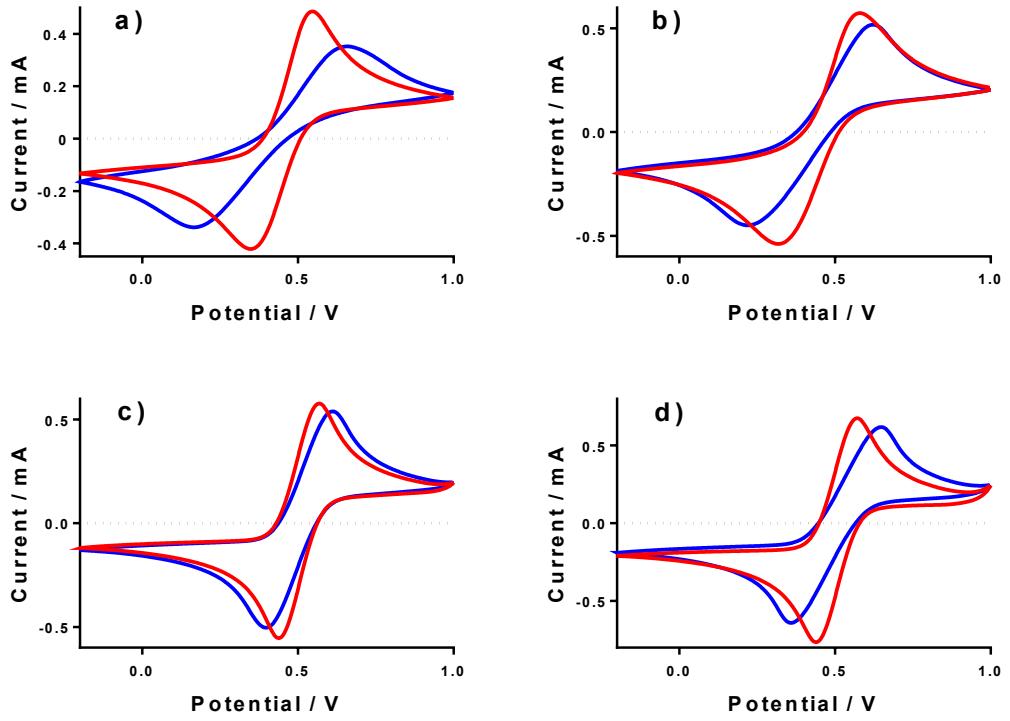

Figure 7 - Cyclic Voltammagrams recorded for (A) NH_4FeSO_4 (B) $FeSO_4$, (C) $FeCF_3SO_3$ and (D) $FeNO_3$ both in the presence (red) and absence (blue) of 1 M conjugate acid. Recorded using an Au working electrode at 50 mV s^{-1}, *vs* a Ag|AgCl reference electrode.

Impedance spectroscopy was recorded, and fitted using the simplest model possible (Figure S4). From this, two resistance values R_{ET} and R_S were quantified, which broadly represented the resistance for electron transfer (or polarisation resistance) at the electrode surface and the solution resistance, respectively.

Figure 8 displays graphically the (a) solution resistance (R_S), and (b) electron transfer resistance (R_{ET}) for the four systems when measured in the thermoelectrochemical cell at *ca.* 25ºC, with and without addition of acid, actual spectra shown in Figure S5; values listed in Table S4. For comparison, the (c) thermocell resistance for the same systems in the thermogalvanic cell (R_{cell}) at ΔT = 20ºC are shown (values listed in Table S5); these are determined by the gradient of the potential vs current data shown in Figure 6.

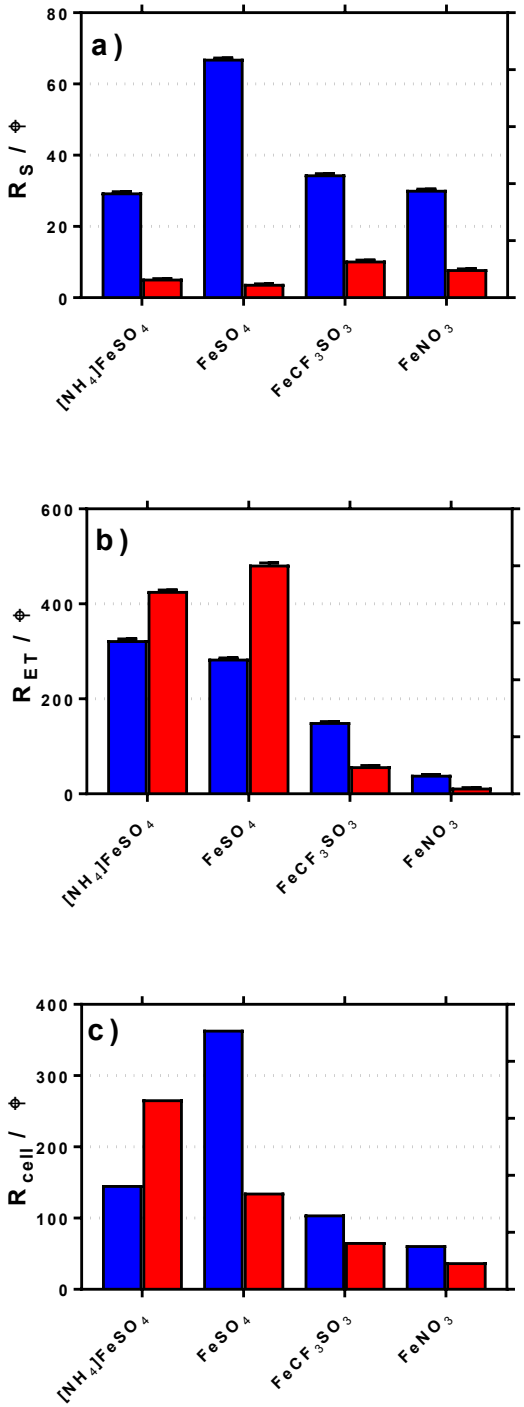

Figure 8 - Plots of the (a) Solution Resistance, R_S and (b) Electron Transfer (or polarisation) Resistance, R_{ET}, determined in the isothermal cell using impedance spectroscopy. Also shown is the (c) Calculated internal resistance of the thermogalvanic cell at $\Delta T = 20°C$, R_{cell}, based upon Ohms Law (V = IR) and the I-V plots shown in Figure 5.

As shown in Figure 8(a), all systems had similar R_s values, which is reasonable considering the concentration of ions present; the higher R_s value for $FeSO_4$ was likely a result of the ion pairing known to occur in this system, while the ion pairing expected for $[NH_4]FeSO_4$ would have been offset by the additional ions present (as $[NH_4]^+$ and $[SO_4]^{2-}$).

All R_s values decreased to negligible values after the addition of 1 M of the conjugate acid, with lower values for the diprotic H_2SO_4-containing systems.

As shown in Figure 8(b), the R_{ET} values were *ca.* 4- to 8-fold higher than the R_S values for the $[NH_4]FeSO_4$, $FeSO_4$ and $FeCF_3SO_3$ systems. Interestingly, $FeNO_3$ demonstrated by far the lowest R_{ET} value, such that it was on par with the R_s value. Additionally, impedance demonstrated that the addition of acid decreased R_{ET} for $FeCF_3SO_3$ and $FeNO_3$, but increased R_{ET} for $[NH_4]FeSO_4$ and $FeSO_4$.

The rate of electron transfer for the Fe(II)/Fe(III) couple is known to be surface-sensitive.[26] For the $FeCF_3SO_3$ and $FeNO_3$ systems, a lower R_{ET} could be due to pH-induced changes of the gold surface, improving electrocatalysis at the gold surface. However, this is counter-intuitive since surface oxides are well known to promote electron transfer constants for the Fe(II)/Fe(III) couple,[26] but be less prevalent at lower pH values.[27] Alternatively, it could simply be a reflection of a change in relative speciation, on par with the increased current observed in Figure 6(c) and (d); more redox species present will reduce R_{ET}. Since R_{ET} was far higher for $[NH_4]FeSO_4$ and $FeSO_4$ than the other two systems, and increased upon acidification, the most likely explanation here is sulphate-poisoning of the gold electrode surface; both $[SO_4]^{2-}$ and $[HSO_4]^-$ anions are known to strongly chemisorb upon gold electrode surfaces, hindering gold oxide formation (relative to $[ClO_4]^-$)[28].

These trends are mirrored somewhat in the R_{cell} values shown in Figure 8(c); the results indicate the thermogalvanic performance of all systems are likely largely controlled by the R_{ET} value;[†] the relatively low R_{ET} value for $FeNO_3$ explains the relatively high power produced by this system. This also allows us to (tentatively) conclude that a drop in R_{cell} for $FeSO_4$ upon acidification is primarily due to a supporting electrolyte-type effect, with the added H_2SO_4 reducing solution resistances and offsetting an increased electrode poisoning effect. In the case of $[NH_4]FeSO_4$, the supporting electrolyte-type effect cannot offset the increase in R_{ET}, such that R_{cell} actually increases. However, despite these changes in R_{cell}, the power output for these two systems actually increased very significantly upon acidification (*cf.* Figure 6); this effect is therefore dominated by the increase in the S_e due to changes in

[†] Impedance measurements of resistance values in an isothermal setup are expected to be different to impedance measurements in a non-isothermal cell. Furthermore, the internal resistance reported for the thermocell represents a steady-state discharge system; here there will be significantly altered redox ratios at the electrode surfaces, and the mass transfer in the thermogalvanic cell often involves more than simple diffusion. Therefore comparison between such impedance measurements and actual thermogalvanic cell performance characteristics need to be approached with caution.

speciation. Since an increased S_e exerts a very significant effect upon the efficiency of the heat-to-current transfer,[16] it results in a higher current as well as a higher potential, both boosting power output. In the case of $FeCF_3SO_3$ and $FeNO_3$, acidification reduces both R_S and R_{ET}; further work is required to identify which of the many components involved in acidification (changed speciation, reduced ohmic drop, changes in surface electrocatalytic sites, *etc.*) are dominant.

Sustainability

Sustainable chemistry generally requires a confluence of economic, societal and 'green' chemistry benefits to be viable.[29] Considering the economic aspects, it is premature to develop a complete technoeconomic model for these systems. However, Table 1 lists the cost in reagents required to fill the thermoelectrochemical cell with 0.4 M of the iron species (full details regarding the reagents, quantity, purchase price, *etc.* are listed in Table S6). It then uses the systems power density at ΔT = 20ºC to present a relative ratio of cost by performance; this value should not be interpreted as cost of power production since no time factor has been included, but is useful to compare the systems.

Table 1 – Preliminary economic comparison of the systems, showing cost per reagent to fill the cell. The ratio of cost to power (£ / W, for $\Delta T = 20°C$) is an arbitrary ratio and represents just one second of measurement; extended use of these cells would reduce this considerably.

Iron redox system	Cost of Fe^{3+} / £ per cell	Cost of Fe^{2+} / £ per cell	Cost of 1 M acid / £ per cell	Total cost per cell / £		Ratio of cost : power (£ / W)	
				Un-acidified	Acidified	Un-acidified	Acidified
$[NH_4]FeSO_4$	0.0047	0.0079	0.0014	0.013	0.014	458	52
$FeSO_4$	0.0067	0.0027	0.0014	0.009	0.011	353	19
$FeCF_3SO_3$	1.86	0.55	0.11	2.414	2.52	1,275	812
$FeNO_3$	0.0058	0.0930*	0.0022	0.099	0.101	33	20

* Cost for $AgNO_3$ and $FeCl_2$

In the absence of acid, it is clear that the moderate cost and high power produced by the $FeNO_3$ system resulted in the best ratio of cost : power by at least one order of magnitude. However, the cells containing $FeSO_4$ and $[NH_4]FeSO_4$ are by far the cheapest; acidification improved the cost : power of the $FeSO_4$ cell more than 20-fold, such that the acidified $FeSO_4$ cell became the most cost effective. Despite the relatively good power produced by the $FeCF_3SO_3$ system, the high cost (especially of the Fe(III) salt) resulted in this system having by far the worst cost : power ratio. These considerations ignore economy of scale. However, preliminary searches in this area demonstrated that the $FeSO_4$ system was likely to benefit most from this, with this material on sale on the kg scale at *ca.* 100-fold less on a £ per gram basis.[‡]

The 12 principles of green chemistry[30] provide some categories against which the four different systems can be assessed. However, primarily only principle 4 (designing safer chemicals) and principle 10 (design for degradation) apply.

In considering the need to design safer chemicals, they should maintain functionality while minimising toxicity.[30] Toxicity data was unavailable for the majority of the iron salts, but where available all values fell within the 'moderately toxic' range on the Gosselin, Smith and Hodge oral toxicity rating; the four systems cannot be easily distinguished. The acidified

[‡] At the time of writing, 25 kg of $Fe(II)SO_4$-$7H_2O$ was for sale for £22.95 on ebay.co.uk, as a lawn supplement.

samples are all also dominated by corrosive nature; these represent a more severe risk to safety and again are all essentially equally undesirable properties.

In considering design for degradation, the $[CF_3SO_3]^-$ system fails given the anion is highly fluorinated and there is no evidence of biodegradation occurring.[31] Conversely, $[SO_4]^{2-}$ and $[HSO_4]^-$ are both naturally abundant in all water sources, including tap water;[32]. Both the $[NO_3]^-$ (in $FeNO_3$) and the $[NH_4]^+$ (in $[NH_4]FeSO_4$) are essential parts of a wide range of ecological environments and are technically 'bio-available' rather than biodegradable, but an over-abundance can disrupt the ecology and present long-term risks to humans (via drinking water).[33]

Finally, green chemistry broadly dictates that the systems should be as stable and as safe as possible. Here, $Fe(II)[NO_3]_2$ is notable as it is known to slowly decompose due to oxidation of $[NO_3]^-$ by the Fe^{2+}.[17] This occurs very slowly, but does represent a possible risk to the user (NO_x gas evolution), likely limits the longevity of the $FeNO_3$ system, and is a route *via* which atmospheric pollution is anticipated.

Overall, these points indicate that the acidified $FeSO_4$ represents the most economical and environmentally sustainable system. The higher power generated by the $FeNO_3$ system is only superior if gravimetric or volumetric considerations are included.

Conclusions

This study has investigated four distinct iron salt systems (with different anions) in terms of their thermogalvanic ability to convert a temperature gradient into electrical power. Two systems included the divalent sulphate anion (the $[NH_4]FeSO_4$ and $FeSO_4$ systems); two had weakly coordinating monovalent anions (the $FeNO_3$ and $FeCF_3SO_3$ systems). This resulted in significant differences between these systems, with the sulphate-based systems demonstrating strong pH sensitivity, and extensive ion pairing resulted in orders of magnitude less thermogalvanic power being generated compared to the monovalent systems. The monovalent anion systems were more strongly influenced by the dissociation of water of hydration rather than ion pairing. A fifth system, iron chloride, did not yield stable results under the conditions used in this study.

This study has also demonstrated that addition of sulphuric acid to the thermogalvanic cell was beneficial in terms of speciation and also a supporting electrolyte-type effect (to

reduce internal ohmic resistances) but was detrimental to the electron transfer resistance. Conversely, the conjugate acid of the monovalent anions improved the relative speciation and decreased both bulk and electron transfer resistances, resulting in more power being generated.

A preliminary costing comparison, and an evaluation of the 'green' credentials of the four systems, resulted in the $FeSO_4$ system being clearly identified as the preferred system; conversely, the $FeCF_3SO_3$ system was highlighted as extremely uncompetitive. The $FeNO_3$ was superior in terms of the overall power generated per cell, and these systems investigated were consistently economically competitive (on the scale employed) but does demonstrate potential longevity, safety and environmental issues.

Overall the highly significant role of the anion in the thermogalvanic performance of Fe^{2+}/Fe^{3+}-based systems has been demonstrated. Going forward, non-coordinating monovalent cations that are both cost-effective and environmentally benign need to be identified.

References

1 T. I. Quickenden and Y. Mua, *J. Electrochem. Soc.*, 1995, **142**, 3985.

2 B. Burrows, *J. Electrochem. Soc.*, 1976, **123**, 154–159.

3 S. G. Bratsch, *J. Phys. Chem. Ref. Data*, 1989, **18**, 1–21.

4 A. Gunawan, C.-H. Lin, D. A. Buttry, V. Mujica, R. A. Taylor, R. S. Prasher and P. E. Phelan, *Nanoscale Microscale Thermophys. Eng.*, 2013, **174**, 304–323.

5 M. Al Maimani, J. J. Black and L. Aldous, *Electrochem. Commun.*, 2016, **72**, 181–185.

6 J. J. Black, T. Murphy, R. Atkin, A. Dolan and L. Aldous, *Phys. Chem. Chem. Phys.*, 2016, **18**, 20768–20777.

7 J. J. Black, A. Dolan, J. B. Harper and L. Aldous, *Phys. Chem. Chem. Phys.*, 2018, **20**, 16558–16567.

8 A. Gunawan, H. Li, C.-H. Lin, D. A. Buttry, V. Mujica, R. A. Taylor, R. S. Prasher and P. E. Phelan, *Int. J. Heat Mass Transf.*, 2014, **78**, 423–434.

9 C. Lin, A. Gunawan, P. E. Phelan, D. A. Buttry and R. A. Taylor, *ASME Proceedings*, 2012, **6**, 541-547, doi:10.1115/IMECE2012-88796.

10 P. Yang, K. Liu, Q. Chen, X. Mo, Y. Zhou, S. Li, G. Feng and J. Zhou, *Angew. Chem. Int. Ed.*, 2016, **55**, 12050–12053.

11 N. Sutin, M. J. Weaver and E. L. Yee, *Inorg. Chem.*, 1980, **19**, 1096–1098.

12 T. Migita, N. Tachikawa, Y. Katayama and T. Miura, *Electrochemistry*, 2009, **77**, 639–641.

13 L. Zhang, T. Kim, N. Li, T. J. Kang, J. Chen, J. M. Pringle, M. Zhang, A. H. Kazim, S. Fang, C. Haines, D. Al-Masri, B. A. Cola, J. M. Razal, J. Di, S. Beirne, D. R. MacFarlane, A. Gonzalez-Martin, S. Mathew, Y. H. Kim, G. Wallace and R. H. Baughman, *Adv. Mater.*, 2017, **29**, 1–7.

14 Y. Yamato, Y. Katayama and T. Miura, *ECS Trans.*, 2012, **50**, 167–174.

15 E. H. B. Anari, M. Romano, W. X. Teh, J. J. Black, E. Jiang, J. Chen, T. Q. To, J. Panchompoo and L. Aldous, *Chem. Commun.*, 2016, **52**, 745–748.

16 L. Aldous, J. J. Black, M. C. Elias, B. Gélinas and D. Rochefort, *Phys. Chem. Chem. Phys.*, 2017, **19**, 24255–24263.

17 C. J. Ottley, W. Davison and W. M. Edmunds, *Geochim. Cosmochim. Acta*, 1997, **61**, 1819–1828.

18 J. Wu, J. J. Black and L. Aldous, *Electrochim. Acta*, 2017, **225**, 482–492.

19 M. S. Romano, S. Gambhir, J. M. Razal, A. Gestos, G. G. Wallace and J. Chen, *J. Therm. Anal. Calorim.*, 2012, **109**, 1229–1235.

20 E. L. Yee, R. J. Cave, K. L. Guyer, P. D. Tyma and M. J. Weaver, *React. Entropies Transit. Met. Redox Couples A*, 1979, **101**, 1131–1137.

21 J. Majzlan and S. C. B. Myneni, *Environ. Sci. Technol.*, 2005, **39**, 188–194.

22 C. C. Loures, M. A. K. Alcântara, H. J. Izario Filho, A. C. S. C. Teixeira, F. T. Silva, T. C. B. Paiva and G. R. L. Samanamud, *Int. Rev. Chem. Eng.*, 2013, **5**, 102–120.

23 R. Diaz-Torrez and S. Alvarez, *Dalt. Trans.*, 2011, **40**, 10742–10750.

24 D. H. Ripin and D. A. Evans, pKa's of Inorganic and Oxo-Acids, http://ccc.chem.pitt.edu/wipf/MechOMs/evans_pKa_table (accessed 13th August 2018).

25 F. G. Bordwell, *Acc. Chem. Res.*, 1988, **21**, 456–463.

26 R. L. McCreery, *Chem. Rev.*, 2008, **108**, 2646–2687.

27 L. Aldous and R. G. Compton, *Phys. Chem. Chem. Phys.*, 2011, **13**, 5279–5287.

28 H. Angerstein-Kozlowska, B. E. Conway, A. Hamelin and L. Stoicoviciu, *J. Electroanal. Chem.*, 1987, **228**, 429–453.

29 M. Philippe, B. Didillon and L. Gilbert, *Green Chem.*, 2012, **14**, 952–956.

30 P. Anastas and J. Warner, *Green Chemistry: Theory and Practice*, Oxford University Press, Oxford [England], 2000.

31 D. Coleman and N. Gathergood, *Chem. Soc. Rev.*, 2010, **39**, 600–637.

32 Sulfate in Drinking-water: Background document for development of WHO Guidelines for Drinking-water Quality (WHO/SDE/WSH/03.04/114), http://www.who.int/water_sanitation_health/dwq/chemicals/sulfate.pdf (accessed 16th July 2018)

33 Y. Xue, J. Song, Y. Zhang, F. Kong, M. Wen and G. Zhang, *Water*, 2016, 8(8), 328.